B-meson hadroproduction in the SACOT-m_{T} scheme

Ilkka Helenius and Hannu Paukkunen

University of Jyvaskyla, Department of Physics,
P.O. Box 35, FI-40014 University of Jyvaskyla, Finland
Helsinki Institute of Physics,
P.O. Box 64, FI-00014 University of Helsinki, Finland

E-mail: ilkka.m.helenius@jyu.fi, hannu.paukkunen@jyu.fi

ABSTRACT: We apply the SACOT-m_{T} general-mass variable flavour number scheme (GM-VFNS) to the inclusive B-meson production in hadronic collisions at next-to-leading order in perturbative Quantum Chromodynamics. In the GM-VFNS approach one matches the fixed-order heavy-quark production cross sections, accurate at low transverse momentum (p_{T}), with the zero-mass cross sections, accurate at high p_{T}. The physics idea of the SACOT-m_{T} scheme is to do this by accounting for the finite momentum transfer required to create a heavy quark-antiquark pair throughout the calculation. We compare our results with the latest LHC data from proton-proton and proton-lead collisions finding a very good agreement within the estimated theoretical uncertainties. We discuss also scheme-related differences and their impact on the scale uncertainties.

Contents

1 Introduction

The production of mesons containing a bottom quark — collectively called B mesons — in hadronic collisions provides a useful way to study various aspects of Quantum Chromodynamics (QCD). On one hand, thanks to the large bottom quark mass $m_\text{b} \approx 4 \ldots 5\,\text{GeV}$, the perturbative expansion in powers of the strong QCD coupling α_s can be expected to converge relatively well and thereby provide an accurate description of the production mechanism [1–5]. In comparison to charm-quark production where the possible non-perturbative intrinsic charm-quark content of the nucleons [6–8] can stir the interpretation, the bottom-quark production can be seen to be a cleaner process to test the perturbative QCD, though an intrinsic bottom-quark component is not excluded [9, 10]. The B-meson production is sensitive especially to the gluon content of the colliding hadrons and can thus be used to provide information on their non-perturbative structure, the parton distribution functions (PDFs) [11–14]. While the B-meson production is not used as a constraint in the current global fits of proton PDFs [15–17], it should be mentioned that e.g. in comparison to the jet production [18, 19] — a commonly used strong gluon constraint — no external corrections due to multi-parton interactions or hadronization need to be supplied but the entire process can be calculated within the collinear factorization. As a result, the B-meson production could provide a rather clean probe for gluon distributions relying solely on inclusive single-particle production. On the other hand, for observables like the Drell-Yan dilepton or direct W$^\pm$ production the weak decays of heavy-flavoured mesons also produce a significant background of charged leptons whose subtraction requires an accurate theoretical understanding of the heavy-quark production [20]. Analyzing B-meson production in proton-nucleus collisions could provide further constraints for nuclear PDFs and, in the context of heavy-ion collisions, the B-mesons can also be used as a probe of the produced strongly interacting matter [21] and the expected mass hierarchies.

The cross sections for identified B-meson hadroproduction have been measured in several collision systems: proton-antiproton (p-$\overline{\text{p}}$) [22, 23] collisions at Fermilab Tevatron, as well

as in proton-proton (p-p) [24–32], proton-lead (p-Pb) [33, 34], and lead-lead (Pb-Pb) [21] collisions at the Large Hadron Collider (LHC). In many occasions the B-meson cannot be fully reconstructed but only the spectrum of specific decay particles like charged leptons or J/ψ mesons, are measured. In work presented here, we will concentrate exclusively on the reconstructed B mesons, but plan to return to the decay spectra in future publications.

We will discuss the B-meson production mainly in the so-called general-mass variable-flavour-number scheme (GM-VFNS) [35]. The GM-VFNS provides a framework to complement fixed-order QCD calculations with a resummation of heavy-quark mass-dependent logarithms that arise from collinear splitting of partons to heavy quarks. The fixed-order calculations — known to leading order (LO) [1], next-to-LO (NLO) [2, 3], and next-to-NLO (NNLO) [4, 5] in strong coupling α_s — are based purely on diagrams in which the heavy quarks are explicitly excited from massless partons. The resummed parts account for the possibility that the heavy quarks are produced through higher-order diagrams within the initial- and final-state radiation. Although formally suppressed by extra powers of α_s these contributions arise from collinear configurations which are logarithmically enhanced at large values of transverse momenta (p_T). The division between the explicit and shower-originating heavy-quark production channels is not unique which induces a scheme and scale dependence on the description.

Historically, the first variant of GM-VFNS for heavy-flavour hadroproduction was the so-called FONLL (Fixed-Order Next-to-Leading Logarithm) scheme introduced in ref. [36]. Later on the SACOT (Simplified Aivazis-Collins-Olness-Tung) scheme was presented in refs. [37, 38] and has been later on applied e.g. in refs. [39, 40]. In the SACOT scheme, part of the resummed contributions are described by massless partonic coefficient functions which induces an unphysical divergence towards $p_T \to 0$, and one cannot therefore generally extend the calculation down to zero p_T. In refs. [41–43] the authors pointed out that this behaviour can be tamed by suitably tuning the factorization and fragmentation scales. In the FONLL scheme these divergent features are cured by multiplying the zero-mass contributions by a factor $p_T^2/(p_T^2 + c^2 m^2)$, where $c = 5$ by default and m is the heavy-quark mass, which serves to evade the unphysical behaviour while still respecting the principles of GM-VFNS. However, neither of the two is a particularly natural way to cure the divergent behaviour and the former also causes unphysical kinks to the p_T spectrum of heavy-flavoured mesons. Indeed, the reason why the invariant heavy-quark cross section remains finite even at zero p_T is in the mass of the heavy quark which, when properly accounted for, keeps the intermediate particles off-shell — there is always a finite momentum transfer between the colliding, massless initial-state partons. This is the underlying physics idea of the SACOT-m_T scheme which was introduced in ref. [44]. It is the counterpart of the SACOT-χ scheme [45] often used in the context of deeply inelastic scattering. Very recently, preliminary documents of the so-called SACOT-MPS (Massive Phase Space) scheme have also appeared [46, 47], which seems to share partly same ideas as the SACOT-m_T scheme applied in this work.

A somewhat different but closely related approach to heavy-flavour hadroproduction is the one in which fixed-order calculations are matched with a parton shower (FO-PS) [48–51]. This procedure also performs a similar resummation as done in GM-VFNS though it still,

in general, misses part of the resummed contributions that are included in GM-VFNS [44], though it can be used to simulate exclusive final states as well. Also, while it is more natural to use 4-flavour PDFs in the context of FO-PS framework to describe $b\bar{b}$ production (part of the logarithms resummed by the parton shower are included in the evolution of the b-quark PDFs) a consistent use of 5-flavour PDFs is a built-in feature of GM-VFNS making it well-suited for general-purpose PDF studies.

In the present paper our aim is to apply the SACOT-m_T scheme [44], originally devised in the context of D-meson (mesons containing a charm quark) production, to the case of B mesons. The differential cross section $\mathrm{d}\sigma/\mathrm{d}p_\mathrm{T}$ of both D- and B-mesons show a maximum at low p_T but they occur at different values of p_T. How this is linked with the heavy-quark masses is an intrinsic feature of a given scheme and provides thus a well-defined way to study the reliability of different schemes. We also introduce an improved description of the fragmentation variable which evades some difficulties in the original setup. In what follows we will first introduce the formalism in section 2, and then discuss the numerical results in sections 3 and 4 for p-p and p-Pb collisions at the LHC, respectively. In section 5 we summarize the paper discussing our future plans.

2 The SACOT-m_T framework

We will now recapitulate our SACOT-m_T framework [44] for single-inclusive heavy-flavoured meson production in hadronic collisions. The process we study is,

$$h_1(P_1) + h_2(P_2) \longrightarrow h_3(P_3) + X \,,$$

where h_1 and h_2 denote the colliding hadrons and h_3 is the heavy-flavoured meson. The momenta of the hadrons are indicated by P_i. We can write the invariant cross section as

$$\frac{\mathrm{d}^3\sigma^{h_1+h_2\to h_3+X}}{\mathrm{d}^3 P_3/P_3^0} = \sum_{ijk} \int_{z^{\min}}^1 \frac{\mathrm{d}z}{z^2} \int_{x_1^{\min}}^1 \mathrm{d}x_1 \int_{x_2^{\min}}^1 \mathrm{d}x_2\, f_i^{h_1}(x_1,\mu_{\mathrm{fact}}^2)\, f_j^{h_2}(x_2,\mu_{\mathrm{fact}}^2)\, D_{k\to h_3}(z,\mu_{\mathrm{frag}}^2)$$

$$\times J(\vec{p},\vec{P}) \times \frac{\mathrm{d}^3\hat{\sigma}^{ij\to k+X}(\tau_1,\tau_2,\rho,\sqrt{s},\mu_{\mathrm{ren}}^2,\mu_{\mathrm{fact}}^2,\mu_{\mathrm{frag}}^2)}{\mathrm{d}^3 p_3/p_3^0} \tag{2.1}$$

$$-\,\mathrm{subtractions}\,.$$

Here, $d\hat{\sigma}^{ij\to k+X}/d^3 p_3$ are the inclusive partonic cross section for producing a parton k carrying a momentum p_3 in collisions of partons i and j with momenta $p_1 = x_1 P_1$ and $p_2 = x_2 P_2$ in our scheme. The fragmentation of the produced parton k into a heavy-flavoured meson is described by the fragmention functions (FFs) $D_{k\to h_3}(z,\mu_{\mathrm{frag}}^2)$ which depend on the fragmentation scale μ_{frag}^2. The fluxes of partons from the initial-state hadrons are described by the PDFs $f_i(x,\mu_{\mathrm{fact}}^2)$ and they depend on the factorization scale μ_{fact}^2. The subtraction terms are required in order avoid the double counting between the same logarithmic terms that appear in partonic cross sections and PDFs/FFs, as will be discussed later on.

The invariants τ_1, τ_2, and ρ are defined by

$$\tau_1 \equiv \frac{p_1 \cdot p_3}{p_1 \cdot p_2} = \frac{m_\mathrm{T} e^{-y}}{x_2\sqrt{s}}\,, \qquad \tau_2 \equiv \frac{p_2 \cdot p_3}{p_1 \cdot p_2} = \frac{m_\mathrm{T} e^{y}}{x_1\sqrt{s}}\,, \qquad \rho \equiv \frac{m^2}{x_1 x_2 s}\,, \tag{2.2}$$

where $m_T = \sqrt{p_T^2 + m^2}$ and y denote the transverse mass and rapidity of the parton k. Here, p_T is the partonic transverse momentum and m is the heavy-quark mass. The integration limits $x_{1,2}^{\min}$ are

$$x_1^{\min} = \frac{m_T \, e^y}{\sqrt{s} - m_T \, e^{-y}}, \qquad x_2^{\min} = \frac{x_1 m_T \, e^{-y}}{x_1 \sqrt{s} - m_T \, e^y} \,. \tag{2.3}$$

The transverse momentum P_T and rapidity Y of the heavy-flavoured meson are related to the corresponding partonic quantities through the definition of the fragmentation variable z, for which we now use

$$z \equiv \frac{P_3 \cdot (P_1 - P_2)}{p_3 \cdot (P_1 - P_2)} \xrightarrow{\text{c.m. frame}} \frac{P_T}{p_T} = \frac{|\vec{P}|}{|\vec{p}|} \,, \tag{2.4}$$

where we have assumed that the fragmentation is collinear in the center-of-mass (c.m.) frame of the collision. This definition of z is associated with the Jacobian factor in eq. (2.1),

$$J(\vec{p}, \vec{P}) = \sqrt{\frac{\vec{P}_3^2 + M^2}{\vec{P}_3^2} \frac{\vec{p}_3^2}{\vec{p}_3^2 + m^2}} \,, \tag{2.5}$$

where M is the meson mass, and the integration limit $z^{\min}$ is

$$z^{\min} = \frac{|\vec{P}_3|}{\sqrt{s/4 - m^2}} \,. \tag{2.6}$$

We note that the definition of the fragmentation variable z in eq. (2.4) is a little different than the definition our earlier work [44] where we defined the fragmentation variable as $z' \equiv P_3 \cdot (P_1 + P_2)/p_3 \cdot (P_1 + P_2)$. In the c.m. frame this corresponds to the fraction of the heavy-quark energy carried by the meson, $z' = E_{\text{meson}}/E_Q$. The problem of this definition is best visible when $Y = y = 0$, i.e. $z' = M_T/m_T$. The fragmentation functions are zero for $z' \geq 1$, which means that the partonic p_T has a lower limit $p_T^2 \geq P_T^2 + M^2 - m^2 \geq M^2 - m^2$. In other words, heavy quarks at sufficiently low transverse momenta will not form heavy-flavoured mesons at all. The definition of eq. (2.4) evades this problem but also other choices are possible [41, 52]. An issue like this admittedly falls outside the predictive power of collinear factorization and can be categorized as modeling the higher-twist effects associated with the hadronization. We have checked that for the results presented in the present paper, the differences between the two above versions of the fragmentation variable, z and z', remains at most $\sim 10\%$ at small values of p_T — well below the uncertainties originating e.g. from the scale choices — and vanish completely at larger values of p_T.

The partonic cross sections $d\hat{\sigma}^{ij \to k+X}$ in GM-VFNS are subject to a scheme dependence [35] to accomplish a description valid at any p_T. In the SACOT-m_T scheme [44] the processes in which the heavy quarks are explicitly produced from massless flavours,

$$gg \to Q + X \,, \qquad qg \to Q + X \,, \qquad qq \to Q + X \,,$$

are evaluated with partonic cross sections carrying the full heavy-quark mass dependence [3], renormalized in the $\overline{\text{MS}}$ scheme (see Section 3 of ref. [36]). We will refer to these channels

as being the "direct" ones. These fixed-order NLO cross sections contain logarithmic terms $\log \rho$ which originate from (i) collinear radiation of gluons off a final-state heavy quark, (ii) collinear splitting of final-state gluons into a heavy quark-antiquark pair, and (iii) collinear splitting of initial-state gluons into a pair of heavy quark and antiquark. These logarithms can be resummed into the scale dependence of the heavy-quark PDFs $f_Q(x, \mu_{\text{fact}}^2)$ and parton-to-meson FFs, $D_{k \to h_3}(z, \mu_{\text{frag}}^2)$. The resummation then gives rise to the contributions (i) with heavy quarks in the initial state and (ii) in which the fragmentation is initiated by a light parton. We will refer to these channels as being the "non-direct" ones. In our scheme, these processes are evaluated with the zero-mass (ZM) $\overline{\text{MS}}$ expressions for the partonic cross sections $d\hat{\sigma}^{ij \to k+X}(\tau_1^0, \tau_2^0)|_{\text{ZM}}$ [53], where

$$\tau_1^0 = \frac{p_{\text{T}} e^{-y}}{x_2 \sqrt{s}}, \qquad \tau_2^0 = \frac{p_{\text{T}} e^y}{x_1 \sqrt{s}}, \tag{2.7}$$

but replacing the massless variables τ_1^0 and τ_2^0 by the massive invariants τ_1 and τ_2 defined in eq. (2.2). In summary,

Direct:

$$\left. \frac{\mathrm{d}^3 \hat{\sigma}^{ij \to k+X}}{\mathrm{d}^2 p_{\text{T}} \mathrm{d}y} \right|_{\text{SACOT}-m_{\text{T}}} \equiv \frac{\mathrm{d}^3 \hat{\sigma}^{ij \to k+X}(\tau_1, \tau_2, \rho)}{\mathrm{d}^2 p_{\text{T}} \mathrm{d}y}, \qquad ij \to k+X \in \begin{cases} gg \to Q+X \\ qg \to Q+X \\ qq \to Q+X \end{cases} \tag{2.8}$$

Non-direct:

$$\left. \frac{\mathrm{d}^3 \hat{\sigma}^{ij \to k+X}}{\mathrm{d}^2 p_{\text{T}} \mathrm{d}y} \right|_{\text{SACOT}-m_{\text{T}}} \equiv \left. \frac{\mathrm{d}^3 \hat{\sigma}^{ij \to k+X}(\tau_1, \tau_2)}{\mathrm{d}^2 p_{\text{T}} \mathrm{d}y} \right|_{\text{ZM}}, \qquad ij \to k+X \notin \begin{cases} gg \to Q+X \\ qg \to Q+X \\ qq \to Q+X \end{cases} \tag{2.9}$$

To motivate the latter choice we note that to (i) retain the Lorentz invariance, and (ii) recover the zero-mass $\overline{\text{MS}}$ result in the $p_{\text{T}} \to \infty$ limit, eq. (2.9) is a rather natural choice. It implicitly accounts for the fact that even in an apparently massless production channels like $gg \to g(\to Q\overline{Q}) + X$, the final-state parton will eventually split into a heavy quark-antiquark pair such that the relevant variables to describe the underlying process are the massive invariants $\tau_{1,2}$, not the massless ones $\tau_{1,2}^0$ to account for finite virtualities of the intermediate partons. This choice also ensures that the cross sections remain finite in the $p_{\text{T}} \to 0$ limit.

The subtractions in eq. (2.1) associated with the initial-state radiation are obtained by replacing the heavy-quark PDFs $f_Q(x, \mu_{\text{fact}}^2)$ by

$$f_Q(x, \mu_{\text{fact}}^2) \longrightarrow \left(\frac{\alpha_s}{2\pi} \right) \log \left(\frac{\mu_{\text{fact}}^2}{m^2} \right) \int_x^1 \frac{dz}{z} P_{qg} \left(\frac{x}{z} \right) f_g(z, \mu_{\text{fact}}^2) \tag{2.10}$$

$$P_{qg}(z) = \frac{1}{2} \Big[z^2 + (1-z)^2 \Big] \tag{2.11}$$

in the

$$Qg \to Q+X, \quad Qq \to Q+X,$$

channels, and keeping terms up to α_s^3. Similarly, the subtractions associated with the final-state radiation are obtained by replacing the FFs by

$$D_{Q \to h_3}(x, \mu_{\text{frag}}^2) \longrightarrow \left(\frac{\alpha_s}{2\pi}\right) \int_x^1 \frac{dz}{z} d_{QQ}\left(\frac{x}{z}\right) D_{Q \to h_3}(z, \mu_{\text{frag}}^2), \qquad (2.12)$$

$$D_{g \to h_3}(x, \mu_{\text{frag}}^2) \longrightarrow \left(\frac{\alpha_s}{2\pi}\right) \log\left(\frac{\mu_{\text{frag}}^2}{m^2}\right) \int_x^1 \frac{dz}{z} P_{qg}\left(\frac{x}{z}\right) D_{Q \to h_3}(z, \mu_{\text{frag}}^2), \qquad (2.13)$$

$$d_{QQ}(z) = C_f \left\{\frac{1+z^2}{1-z}\left[\log\left(\frac{\mu_{\text{frag}}^2}{m^2}\right) - 2\log(1-z) - 1\right]\right\}_+, \qquad (2.14)$$

in the

$$gg \to Q + X, \qquad qg \to Q + X, \qquad qq \to Q + X,$$
$$gg \to g + X, \qquad qg \to g + X, \qquad qq \to g + X,$$

channels, and keeping terms up to α_s^3. The non-logarithmic terms in d_{QQ} are associated with the definition of the $\overline{\text{MS}}$ FFs in the presence of a finite quark mass [54, 55]. In addition, the fully massive calculation used to evaluate the direct contributions [3] are renormalized in the so-called decoupling scheme [56] in which the scale dependence of α_s excludes the contributions from heavy-quark loops. To translate the results in the decoupling scheme to the usual $\overline{\text{MS}}$ scheme, additional terms are supplied, see Section 3 of ref. [36].

There are three independent scales involved in our calculation — the renormalization, factorization and fragmentation scales. These are taken to be

$$\mu_i = c_i\sqrt{P_{\text{T}}^2 + m^2}, \qquad (2.15)$$

where m is the heavy-quark mass and our default choice is $c_i = 1$, as in ref. [44]. To chart the dependence of our results on this choice we repeat the calculations by taking $c_i = 0.5, 1, 2$, with a restriction,

$$\frac{1}{2} \leq \frac{\mu_{\text{ren}}}{\mu_{\text{fact}}} \leq 2, \qquad \frac{1}{2} \leq \frac{\mu_{\text{ren}}}{\mu_{\text{frag}}} \leq 2. \qquad (2.16)$$

In total there are then 17 different scale combinations whose envelope we take as the scale uncertainty. We note that the FFs become scale independent for $\mu_{\text{frag}} \leq m$ and only $D_{Q \to h_3}$ is non-zero in this regime. The heavy-quark PDFs are zero for $\mu_{\text{fact}} \leq m$. Consistently, no initial-state subtraction terms are included when $\mu_{\text{fact}} \leq m$, and no final-state subtraction terms are included when $\mu_{\text{frag}} \leq m$.

We take the B-meson FFs from the Kniehl-Kramer-Schienbein-Spiesberger analysis (KKSS08) [39] which fits the SLD [57], OPAL [58], and ALEPH [59] data on B-meson production in e^+e^- annihilation near the Z-boson pole, $\sqrt{s} = M_{\text{Z}}$. Recently, also FFs at NNLO accuracy have become available [60]. It should be noted that in the KKSS08 analysis the bottom mass was taken to be $m_{\text{b,FF}} = 4.5\,\text{GeV}$, which differs from the values employed in the PDFs we will use in our calculations, $m_{\text{b}} = 4.92\,\text{GeV}$ for NNPDF4 [16], and $m_{\text{b}} = 4.75\,\text{GeV}$ for MSHT20 [15]. Since the data in KKSS08 analysis are taken at $\sqrt{s} = M_{\text{Z}}$,

the exact value of the bottom-quark mass used there cannot be very critical. On the other hand, the PDF fits utilize much more data at lower interaction scales and are thus arguably much more sensitive to the quark masses (i.e. changing the input masses changes the PDFs). We thus find it better justified to use the mass values from PDFs in our calculations. To ensure the correct behaviour at the threshold, the final-state subtraction terms as well as e.g. the gluon FFs should vanish at the scale $\mu_{\mathrm{frag}} = m_{\mathrm{b}}$. To enforce this, we always use the scale $\mu^2 = c_i \sqrt{P_{\mathrm{T}}^2 + m_{\mathrm{b,FF}}^2}$ when calling the FFs. In the future, to avoid making such compromises, it would be useful to have the B-meson FFs available with the exact mass values utilized in the global PDF fits. In most of our calculations we will use the NNPDF4 partons [16] which constitute the most recent set. To investigate the mass dependence, we will use a special version of MSHT20, MSHT20NLO_MBRANGE_NF5 [61] which provides PDF fits with different bottom-quark masses including also the one which matches with $m_{\mathrm{b,FF}}$. In the case of p-Pb collisions, we will use the EPPS21 nuclear PDFs [62] (with CT18A baseline proton PDFs [17]) for which $m_{\mathrm{b}} = 4.75 \, \mathrm{GeV}$, and the nNNPDF3.0 nuclear PDFs [63] for which $m_{\mathrm{b}} = 4.92 \, \mathrm{GeV}$.

3 Results for proton-proton collisions

To highlight the key features of the SACOT-m_{T} setup we present, in figure 1, the B$^{\pm}$ cross sections at $\sqrt{s} = 13 \, \mathrm{TeV}$ in the rapidity window $2.5 < Y < 3.0$ together with the experimental data from the LHCb collaboration [32]. The full SACOT-m_{T} calculation follows the data very well and, in particular, reproduces the turnover at $P_{\mathrm{T}} \approx 3 \, \mathrm{GeV}$. The scale uncertainty is shown as the green band which is large at small values of P_{T} but reduces to 10% at highest considered values of P_{T}. To illustrate how the B-meson cross section in our scheme builds from various components, figure 1 also shows separately the contributions of direct terms, subtraction terms, and the non-direct parts in which there are either bottom quark(s) in the initial state or in which the fragmentation proceeds from a light parton. At low P_{T} the direct part clearly dominates and, by construction, is the only contribution at $P_{\mathrm{T}} = 0 \, \mathrm{GeV}$. As P_{T} increases the subtraction terms approximate rather well the full direct contribution and eventually the net contribution of these two becomes rather small. When this happens, the contributions from initial-state heavy quarks and light-parton fragmentation are the dominant ones. With our default choice of scales, this begins to happen already around $P_{\mathrm{T}} \approx m_{\mathrm{b}}$. Arguably, the collinear logarithms $\sim \log\left(p_{\mathrm{T}}^2/m^2\right)$ are not yet particularly large at such values of P_{T} so their resummation should not be a too big of an effect either. However, even if the resummation would not yet be a large effect, the non-direct contributions can be significant as e.g. the $gg \to gg$ matrix element that enters the contribution from gluon fragmentation carries a large colour factor which increases its importance even if the associated logarithm would not yet be particularly large. For $P_{\mathrm{T}} \approx m_{\mathrm{b}}$ and higher, the full calculation is significantly above the direct part. On one hand this is due to the α_s^3 terms in the contributions with initial-state heavy quarks or light-parton fragmentation, which also partly catch the NNLO contributions to the fixed-order calculation which are now known to be important [5]. On the other hand, towards higher values of P_{T} the resummation of the collinear logarithms becomes also gradually
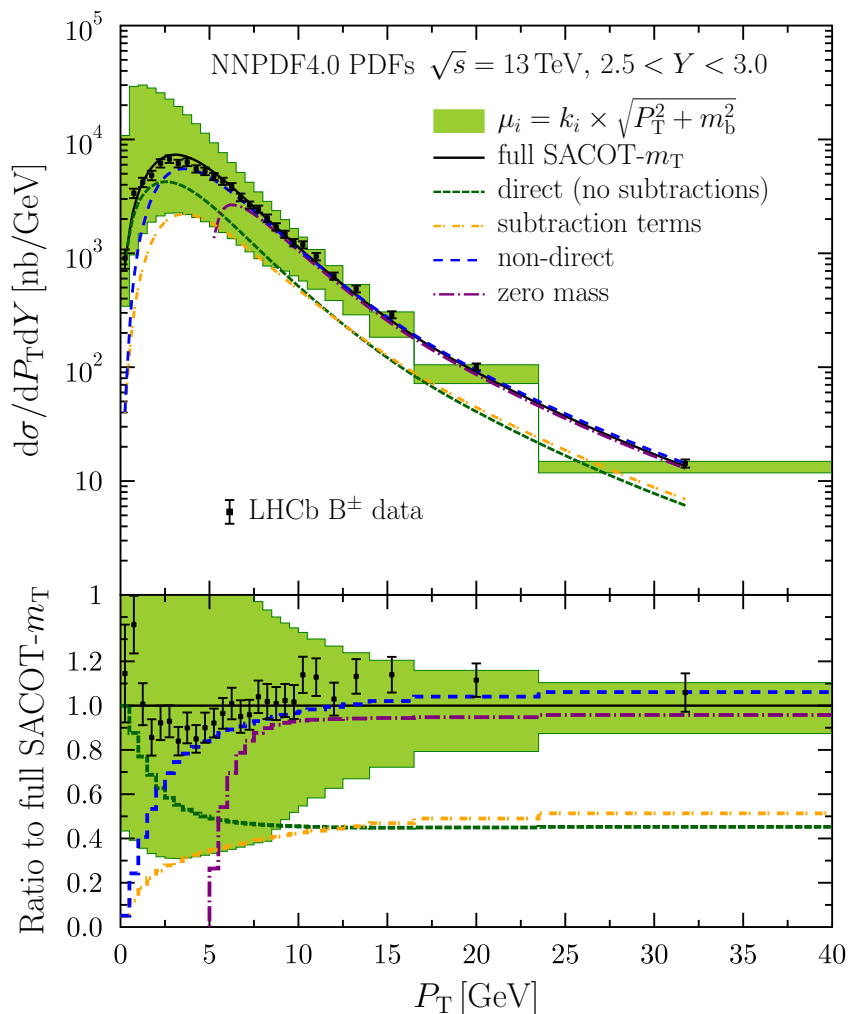
Figure 1. The 13 TeV B$^\pm$-meson data of the LHCb collaboration [32] in the rapidity window $2.5 < Y < 3.0$ compared with the SACOT-$m_{\rm T}$ calculation. The plot shows separately the full calculation (black solid), the direct i.e. light-parton to heavy quark production channels (green dashed), subtraction terms (yellow dotted-dashed), non-direct production channels (blue dashed), and the zero-mass calculation (purple dotted-dashed). The filled bands correspond to the uncertainty from the scale variation.

more important of an effect. The scale variations result in a significant uncertainty band. Part of this largeness is related to the fact that the scale choice also controls the relative importance of the direct, subtraction, and non-direct contributions. For example, with $k_i = 1/2$ only the direct part contributes up to $P_{\rm T} = \sqrt{3}m_{\rm b} \approx 8.5\,{\rm GeV}$, whereas with our default choice of scales it is the non-direct part that clearly dominates at $P_{\rm T} = 8.5\,{\rm GeV}$. The result of a fully zero-mass calculation, but still adopting our default choice of scales, is shown in figure 1 as well. We see that the zero-mass calculation agrees rather well with the full SACOT-$m_{\rm T}$ result already at $P_{\rm T} \gtrsim 2m_{\rm b}$ though the residual mass effects die out rather slowly in $P_{\rm T}$. Towards lower values of $P_{\rm T}$ the NLO zero-mass cross section not only diverges but goes also negative due the spurious behaviour of the zero-mass coefficient functions.
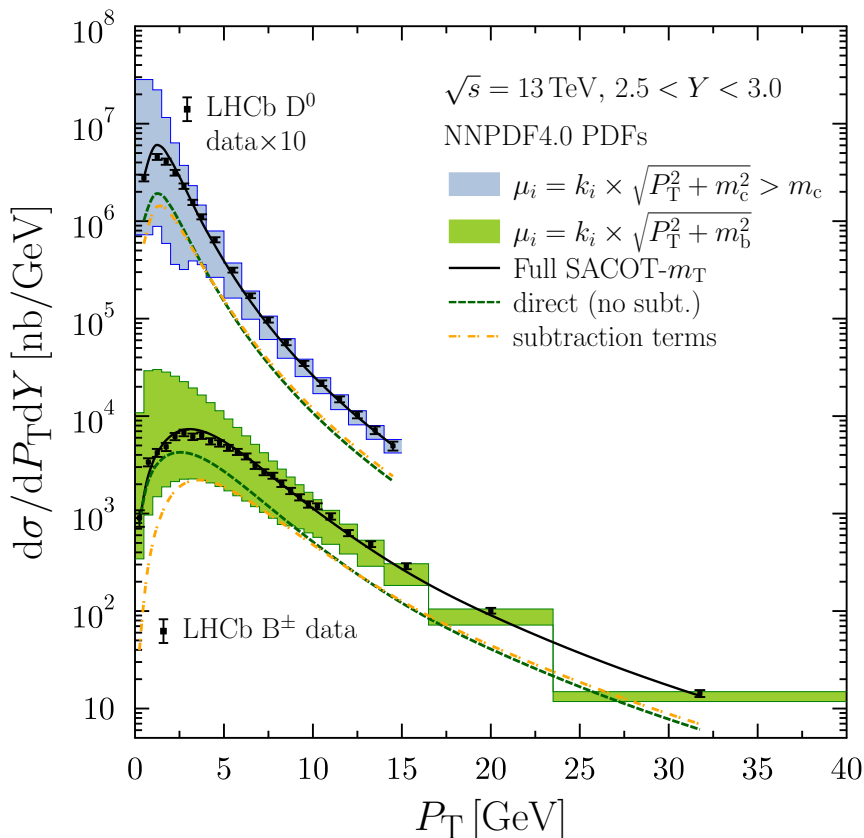
Figure 2. Comparison of D^0- (upper curves) and $B^\pm$-meson (lower curves) production in the SACOT-m_T scheme at $\sqrt{s} = 13\,\text{TeV}$, $2.5 < Y < 3.0$. Black solid curves correspond to the full calculation and the green dashed curves to the contributions from the direct (i.e. light parton to heavy quark) production channels. The orange dashed-dotted curves are the subtraction terms and the filled bands show the uncertainty from the scale variation. The data are from the LHCb collaboration [32, 64]. For clarity, the data and curves corresponding to the D^0 mesons have been multiplied by a factor of 10.

The observations made above are reminiscent of those we found earlier for D mesons [44] but the effects of heavy-quark mass simply persist up to higher values of P_T. This is illustrated in figure 2 where we plot the D^0 results in the same figure. For the D-meson data, the turnover happens at lower P_T in comparison to the B-meson case. This behaviour is also well reproduced by our default scale choice — a larger quark mass more strongly "screens" the partonic propagators due to larger virtuality and shifts the turnover to larger P_T. One can also clearly see that — in our scheme and the default choice of scales — the subtraction terms approximate well the contributions from the direct production channels for D mesons immediately above zero P_T, whereas for B mesons the cancellation between the subtraction terms and the direct production channels is shifted to larger P_T. In comparison to the D-meson results, and perhaps a little surprisingly, the scale uncertainty remains larger for B mesons up to higher P_T although the associated QCD scales are larger. The reason is that for the B-meson production the interplay between various components (direct,
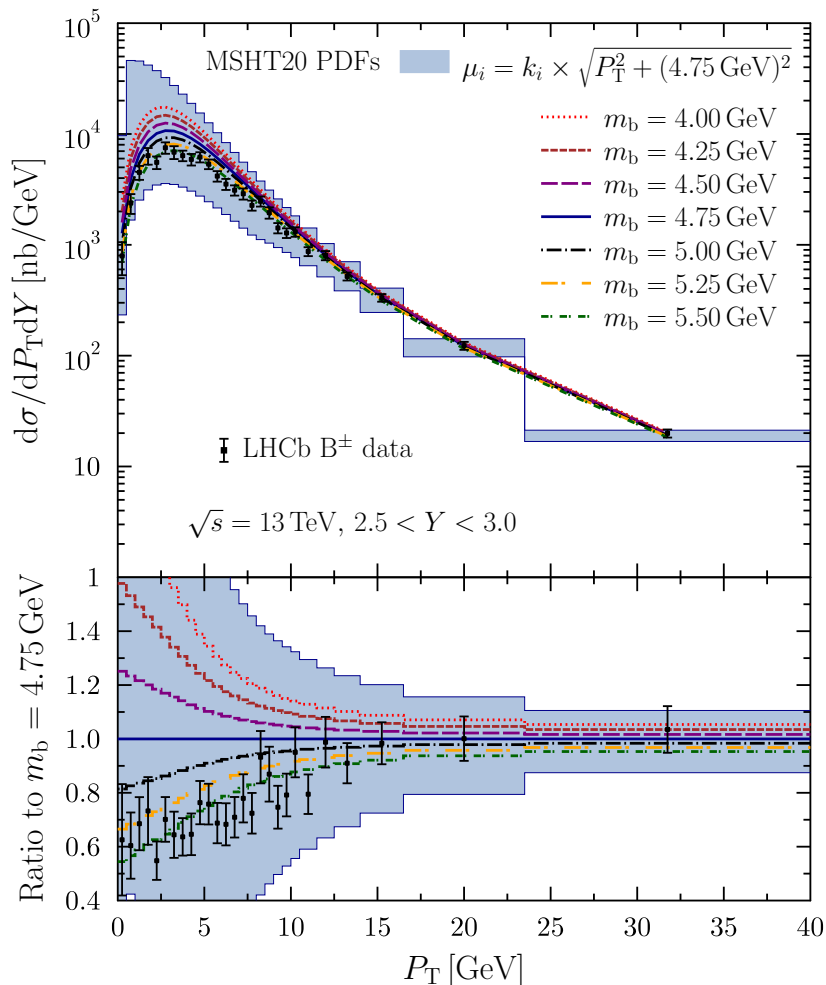
Figure 3. The 13 TeV B$^{\pm}$-meson data of the LHCb collaboration [32] in the rapidity window $2.5 < Y < 3.0$ compared with the SACOT-m_T calculation with different bottom-quark masses m_b. The calculation uses the MSHT20NLO_MBRANGE_NF5 partons [61] which are available for $m_b = 4.0 \ldots 5.50$ GeV. The scale uncertainty band was evaluated with $m_b = 4.75$ GeV.

non-direct, subtraction) remains non-trivial up to higher values of P_T and the dependence of this interplay on the scale choices results in a larger scale uncertainty. In the case of D mesons, the non-direct components quickly dominate the cross section with all considered scale choices. Notice that here we have limited the scales from below by the charm mass to make sure that they stay above the initial scales of the PDF analyses.

The dependence of our calculations on the adopted set of PDFs with different bottom-quark masses is illustrated in figure 3. Instead of NNPDF4.0, we have used here the MSHT20NLO_MBRANGE_NF5 partons [61]. In this latter analysis, the authors repeated the MSHT20 [15] global PDF fit seven times varying the bottom-quark mass in the range $m_b = 4.0 \ldots 5.50$ GeV. By using these PDF sets, we can thus study the bottom-quark dependence of our calculation with the proper behaviour of PDFs (i.e. vanishing bottom-quark) at the threshold $\mu_{\text{fact}} = m_b$. The largest differences appear at low P_T where the
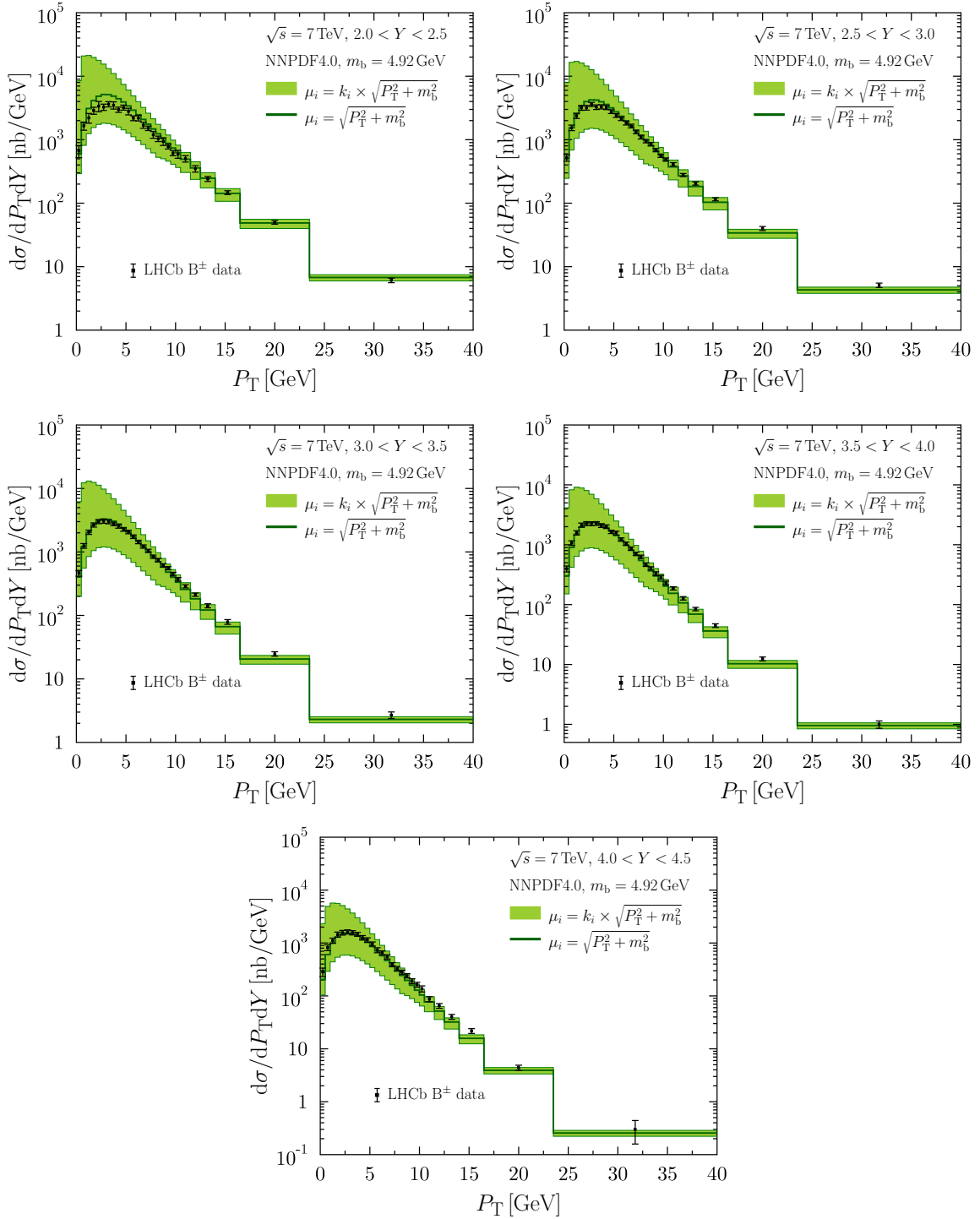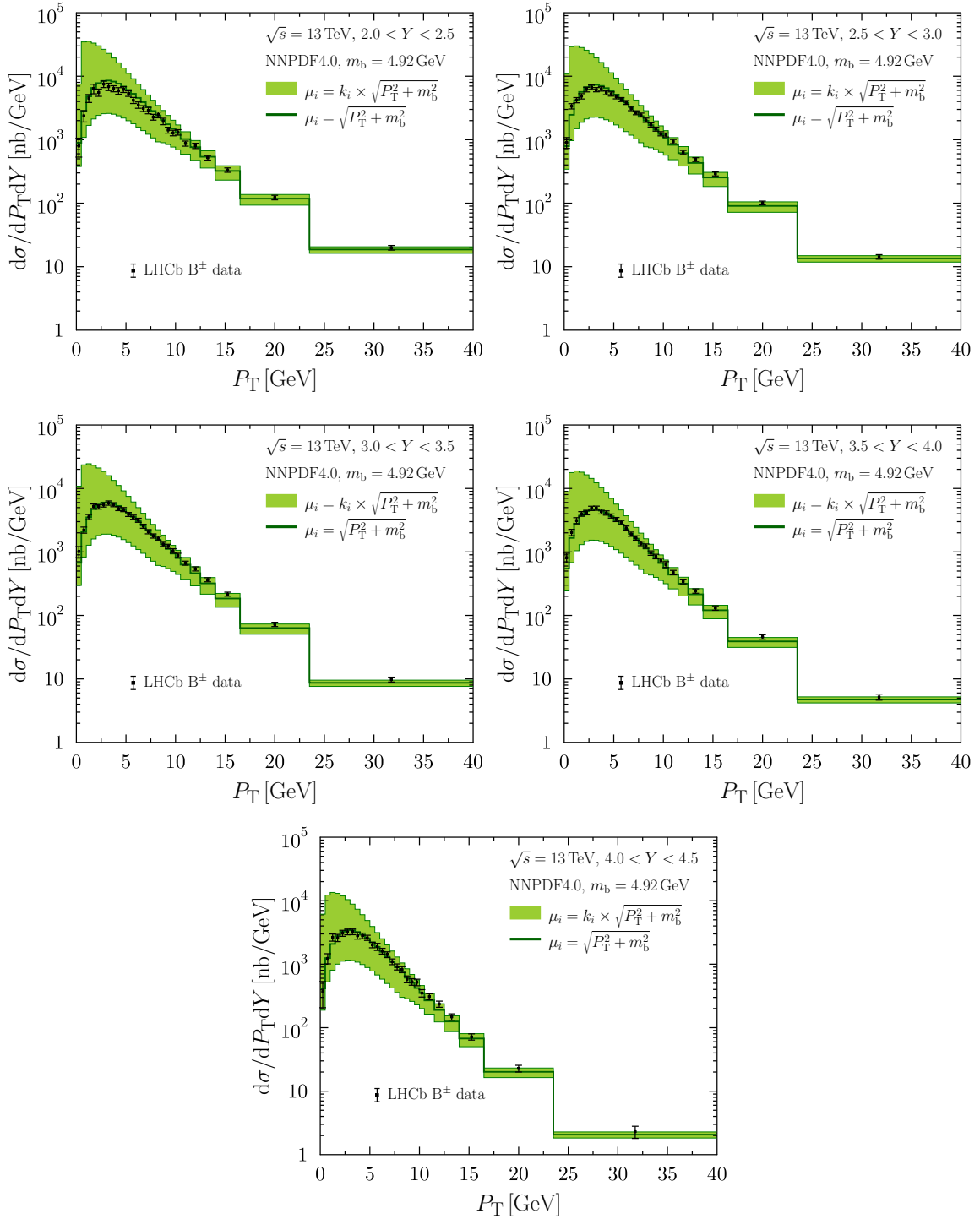
Figure 4. The 7 TeV B$^{\pm}$-meson data of the LHCb collaboration [32] compared with the SACOT-m_{T} calculation. Each panel correspond to a different rapidity window. The green solid curves show the results of our central scale choice $\mu_i = \sqrt{P_{\mathrm{T}}^2 + m_{\mathrm{b}}^2}$, and the light-green filled bands correspond to the uncertainty due to the scale variations.
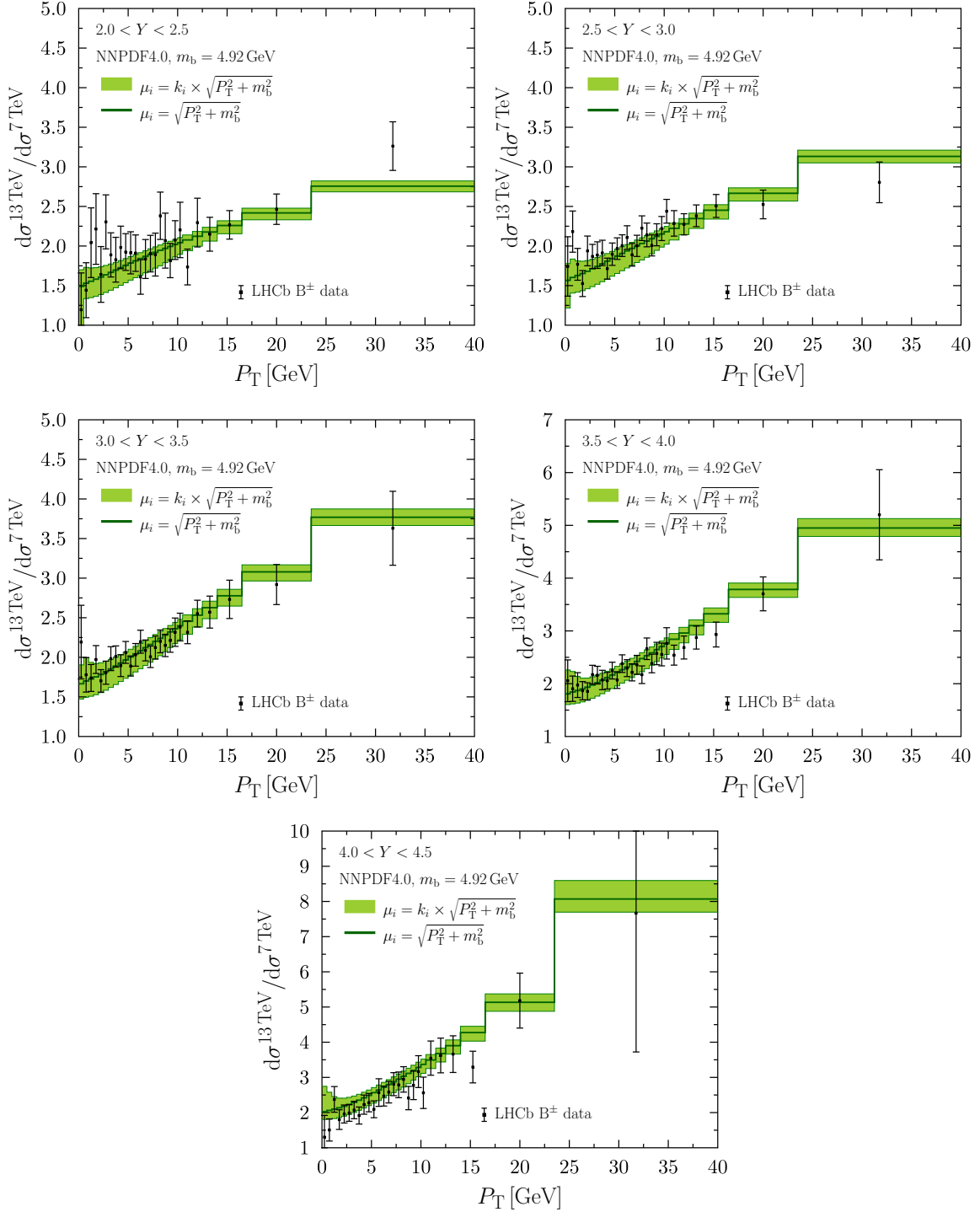
Figure 5. The 13 TeV B$^{\pm}$-meson data of the LHCb collaboration [32] compared with the SACOT-m_{T} calculation. Each panel correspond to a different rapidity window. The green solid curves show the results of our central scale choice $\mu_i = \sqrt{P_{\mathrm{T}}^2 + m_{\mathrm{b}}^2}$, and the light-green filled bands correspond to the uncertainty due to the scale variations.
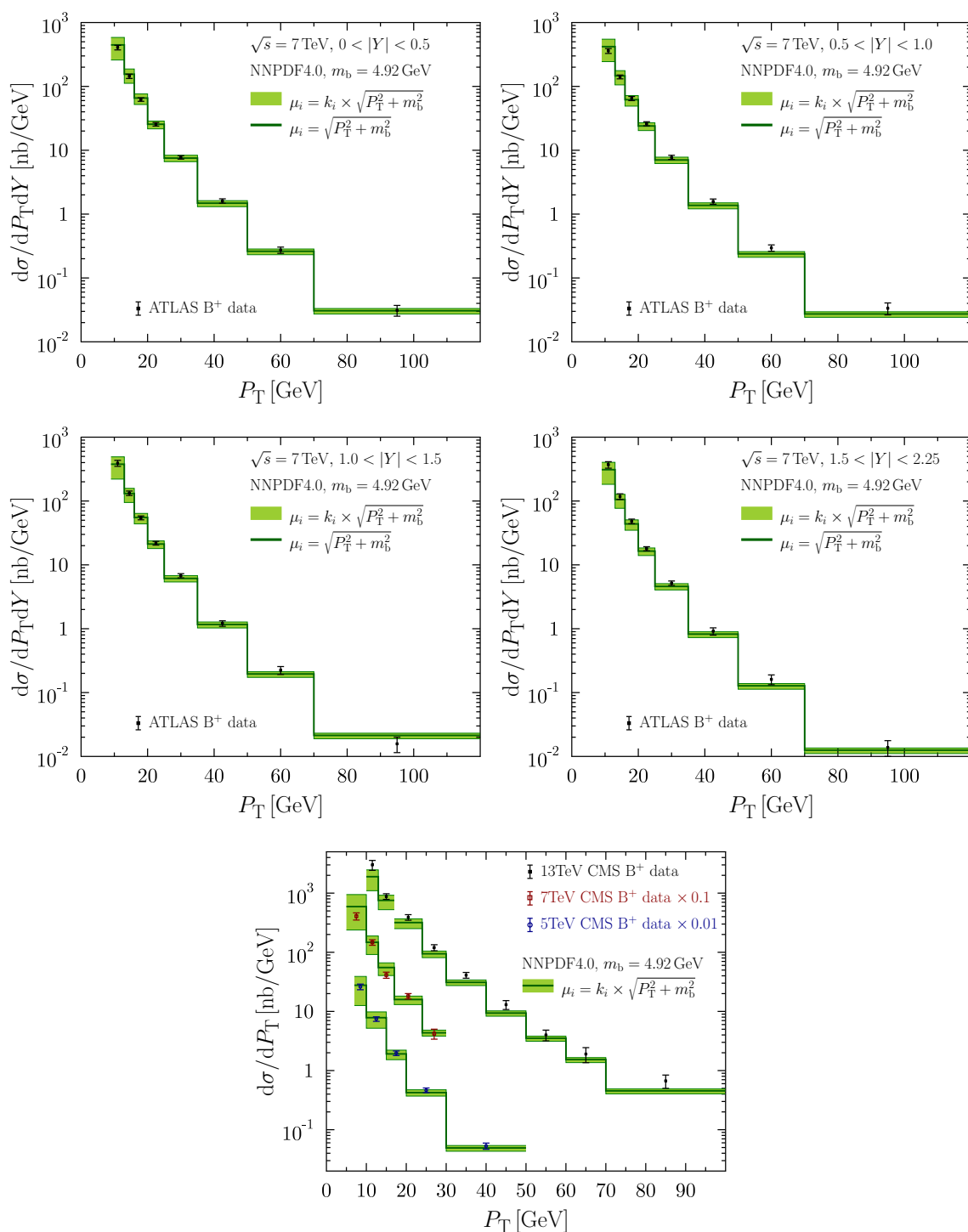
Figure 6. Ratios between the 13 TeV and 7 TeV B$^{\pm}$-meson data of the LHCb collaboration [32] compared with the SACOT-m_{T} calculation. Each panel correspond to a different rapidity window. The green solid curves show the results of our central scale choice $\mu_i = \sqrt{P_{\mathrm{T}}^2 + m_{\mathrm{b}}^2}$, and the light-green filled bands correspond to the uncertainty due to the scale choice.

Figure 7. The 7 TeV B$^{\pm}$-meson data of the ATLAS collaboration [29] (upper panels), and the 5...13 TeV B$^{\pm}$-meson data of the CMS collaboration [21, 25, 30] (lowest panel) compared with the SACOT-m_{T} calculation. Each panel correspond to a different rapidity window. The green solid curves show the results of our central scale choice $\mu_i = \sqrt{P_{\mathrm{T}}^2 + m_{\mathrm{b}}^2}$, and the light-green filled bands correspond to the uncertainty due to the scale choice.

bottom-quark thus plays the most significant role. We see that adopting a smaller bottom-quark mass leads to an increased cross section as the "mass screening" in the propagators decreases. Decreasing the bottom-quark mass can be also seen to slightly shift the maximum of the P_{T} spectrum towards lower values of P_{T}. The mass dependence is still clearly inferior to the scale dependence of our results i.e. within the scale uncertainties all the shown PDFs agree with the LHCb data (note, however, that variations in the mass also affect the scale choices).

Figures 4 and 5 show the comparisons with the LHCb 7 TeV and 13 TeV [32] data using NNPDF4.0 PDFs. In both cases the predictions agree very well with the data throughout the wide rapidity range. The uncertainties from NNPDF4.0 are small (not much larger than the line width) in contrast to the scale uncertainties and are therefore not shown. We consider also the cross section ratios between the collision energies of 13 TeV and 7 TeV. The LHCb paper [32] does not contain these ratios separately for different rapidity bins, and we have therefore formed the ratios ourselves from the tabulated cross sections. The statistical and systematical uncertainties have been added in quadrature apart from the 3.9% systematic uncertainty on the $B^{\pm} \to J/\psi K^{\pm}$ branching fraction (the decay mode measured by the LHCb), which has been canceled out. The results are shown in figure 6. The uncertainties due to the scale choices are vastly smaller in these ratios in comparison to the absolute cross sections. The systematics of the data are well reproduced by the calculation. Despite the smaller scale uncertainties, they are still larger than the PDF-originating uncertainties, at least for NNPDF4.0 which we use here. Finally, figure 7 presents the ATLAS 7 TeV data [29] and the CMS midrapidity data at 5 TeV [21], 7 TeV [25], and 13 TeV [30]. These data do not reach to the low-P_{T} region where most of the bottom-quark mass effects reside but instead extend to higher values of P_{T} and provide therefore a complementary validation of our computational setup. The dependence of experimental cross sections on the c.m. energy, P_{T} and rapidity are again well reproduced by the calculation.

Finally, we wish to illustrate the differences between our SACOT-m_{T} scheme and other approaches. To this end, figure 8 presents a comparison in which we have divided the FONLL [11, 36, 65] and fixed-order NLO calculations with the SACOT-m_{T} predictions. The FONLL and fixed-order NLO predictions have been taken from the web interface in ref. [66] selecting the NNPDF3.0 proton PDFs [67]. The coloured bands show the uncertainties due to the scale variations which, in the case of FONLL and fixer-order calculation, include only variations of the factorization and renormalization scales with 5 different combinations. The FONLL cross section for heavy-quark production is, schematically, of the form,

$$d\sigma_q^{\text{FONLL}} = \sigma^{\text{fixed order}} + \frac{p_{\text{T}}^2}{p_{\text{T}}^2 + c^2 m_q^2} \big(d\sigma^{\text{resummed}} - \text{subtractions} \big) , \qquad (3.1)$$

where the default choice $c = 5$ has been applied, and which is still folded with a scale-independent fragmentation function to obtain the spectrum of heavy-flavoured mesons. While the fixed-order part includes only those contributions in which the heavy quarks are explicitly produced, the resummed part performs the same resummation of collinear logarithms as the SACOT-m_{T} scheme. The subtraction terms ensure that no double counting takes place. The principal difference with respect to the SACOT-m_{T} scheme is
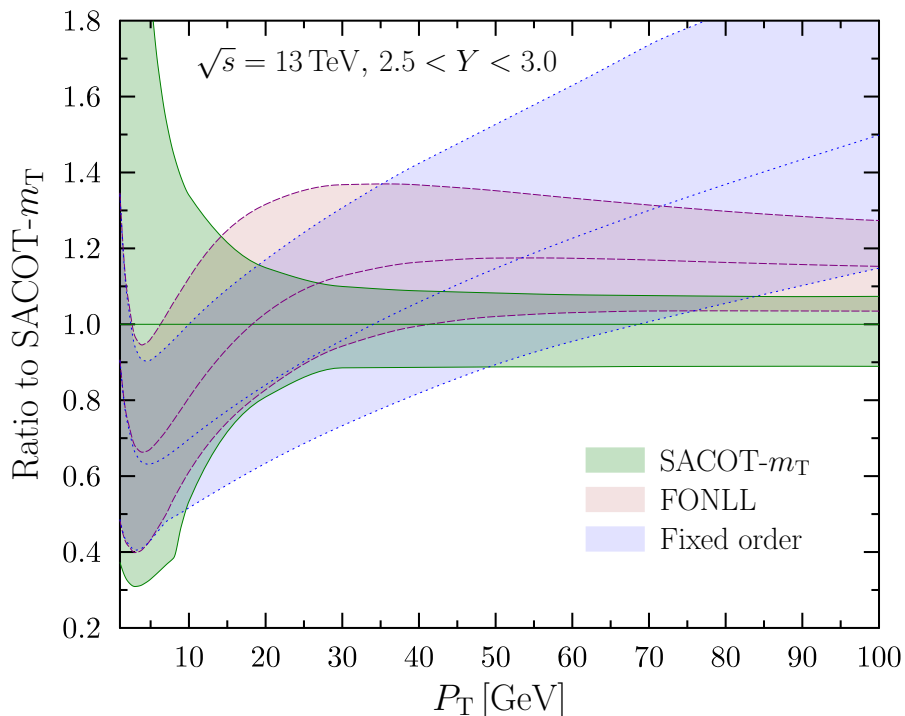
Figure 8. Ratios of FONLL (red band) and fixed-order NLO (blue band) cross sections with respect to the SACOT-m_T calculation (green band) in the rapidity window $2.5 < Y < 3.0$ at $\sqrt{s} = 13\,\text{TeV}$. The FONLL and fixed-order results use the NNPDF3.0 proton PDFs. The widths of the bands correspond to the scale uncertainties of each calculation.

that the resummed part uses pure zero-mass coefficient functions which diverge towards zero p_T. The factor $p_T^2/(p_T^2 + c^2 m_q^2)$ is there to tame the divergence. The constant c controls how quickly the resummation is allowed to kick in as a function of p_T. The default FONLL predictions, however, do not involve an uncertainty due to the variations of the constant c. At low P_T the FONLL predictions match with the fixed-order calculations and show a clearly smaller scale uncertainty in comparison to the SACOT-m_T scheme. This is due to the fact that FONLL suppresses the contributions from the resummed part (which comes with a large scale uncertainty at low P_T) by choosing a large enough c. This is of course well justified in the sense that at low P_T the collinear logarithms are not yet large and thus their resummation cannot be a big effect either. However, we recall that by including the $\mathcal{O}(\alpha_s^3)$ terms in the resummed cross sections, they also effectively contain contributions from the fixed-order NNLO calculations which can be significant even if the resummation of the associated logarithms is not yet crucial. Moving towards somewhat higher values of P_T the scale uncertainty of the SACOT-m_T scheme quickly diminishes and becomes eventually smaller than that of FONLL — starting from $P_T \approx 3m_b$ or so. This indicates that the resummation begins to have an effect at such values of P_T but the chosen value of c in FONLL still retains the fixed-order contribution (with a larger scale uncertainty) significant. At the high-P_T end both FONLL and SACOT-m_T display a scale uncertainty which is approximately the same for both and clearly smaller than the scale uncertainty of the fixed-order predictions.

4 Results for proton-nucleus collisions

The D-meson production in p-Pb collisions [68] has been used as a constraint in the EPPS21 [62] and nNNPDF3.0 [63] fits of nuclear PDFs. The theoretical framework in the EPPS21 analysis was the one discussed here, SACOT-m_T, while the nNNPDF3.0 analysis used a fixed-order POWHEG calculation [48–50] matched to the PYTHIA [69] parton shower. The differences between the two approaches were discussed in ref. [44]. Heavy-flavour observables have also been studied in a recent variant of the nCTEQ15 analysis [70] but using considerable simplifications on the partonic matrix elements and kinematics. Specifically, it is the nuclear modification

$$R_{\mathrm{pPb}} = \frac{d^2\sigma^{\mathrm{p\text{-}Pb}}/dY\,dP_\mathrm{T}}{d^2\sigma^{\mathrm{p\text{-}p}}/dY\,dP_\mathrm{T}}\,, \tag{4.1}$$

for D-meson production that enters the EPPS21 and nNNPDF3.0 analyses. In such ratio most of the scale uncertainties in the SACOT-m_T scheme were observed to cancel between the numerator and denominator though some dependence persist, particularly at low P_T [13]. To be on the safe side, EPPS21 imposed a cut $P_\mathrm{T} > 3\,\mathrm{GeV}$. In the POWHEG+PYTHIA approach the scale uncertainties in R_{pPb} at high P_T were observed to be much larger than in the SACOT-m_T scheme [63]. The nNNPDF3.0 analysis nevertheless included the D-meson data without any restrictions in P_T excluding, however, the p-Pb data at backward rapidities ($Y < 0$). In both cases, the inclusion of the LHCb data [68] led to a significant reduction of the nuclear-PDF uncertainties at small x. In this section we will now use these D-meson-constrained nuclear PDFs to predict the nuclear modification ratios for B-mesons and see whether the predictions agree with the recent LHCb data [34].

Before comparing with the data we study the relative size of the PDF and scale uncertainties in B-meson R_{pPb}. This is done in figure 9 in which the relative scale and 90% PDF uncertainties for R_{pPb} are shown. For EPPS21, the PDF uncertainty is calculated according to the Hessian prescription, see Section 4.3 of ref. [62], whereas the 90% nNNPDF3.0 uncertainty is calculated by rejecting the predictions of those replicas that constitute 10% of the most extreme predictions, see Section 7.2 of ref. [63]. In both cases, the correlations between the nuclear and proton PDFs are accounted for. The full uncertainty band combines the PDF and scale uncertainties in quadrature. The scale uncertainties are the largest at low values of P_T and they are very similar between EPPS21 and nNNPDF3.0. In the case of EPPS21 the PDF uncertainties are always clearly larger than the those induced by the scale variations. The nNNPDF3.0 PDF uncertainties are, however, systematically smaller than those of EPPS21 and in places the scale uncertainty competes and even exceeds the PDF uncertainty. The fact that the nNNPDF3.0 uncertainties are generally smaller than those of EPPS21 is presumably mostly due to the methodological differences between these two PDF analyses [71].

Figure 10 shows how our calculations using the EPPS21 and nNNPDF3.0 nuclear PDFs compare against the LHCb B$^\pm$-meson data at 8.16 TeV [34]. In the backward direction $-3.5 < Y < -2.5$ (Y referring to the rapidity of the meson in nucleon-nucleon center-of-mass frame) one probes predominantly the large-x part of the nuclear PDFs where there is an
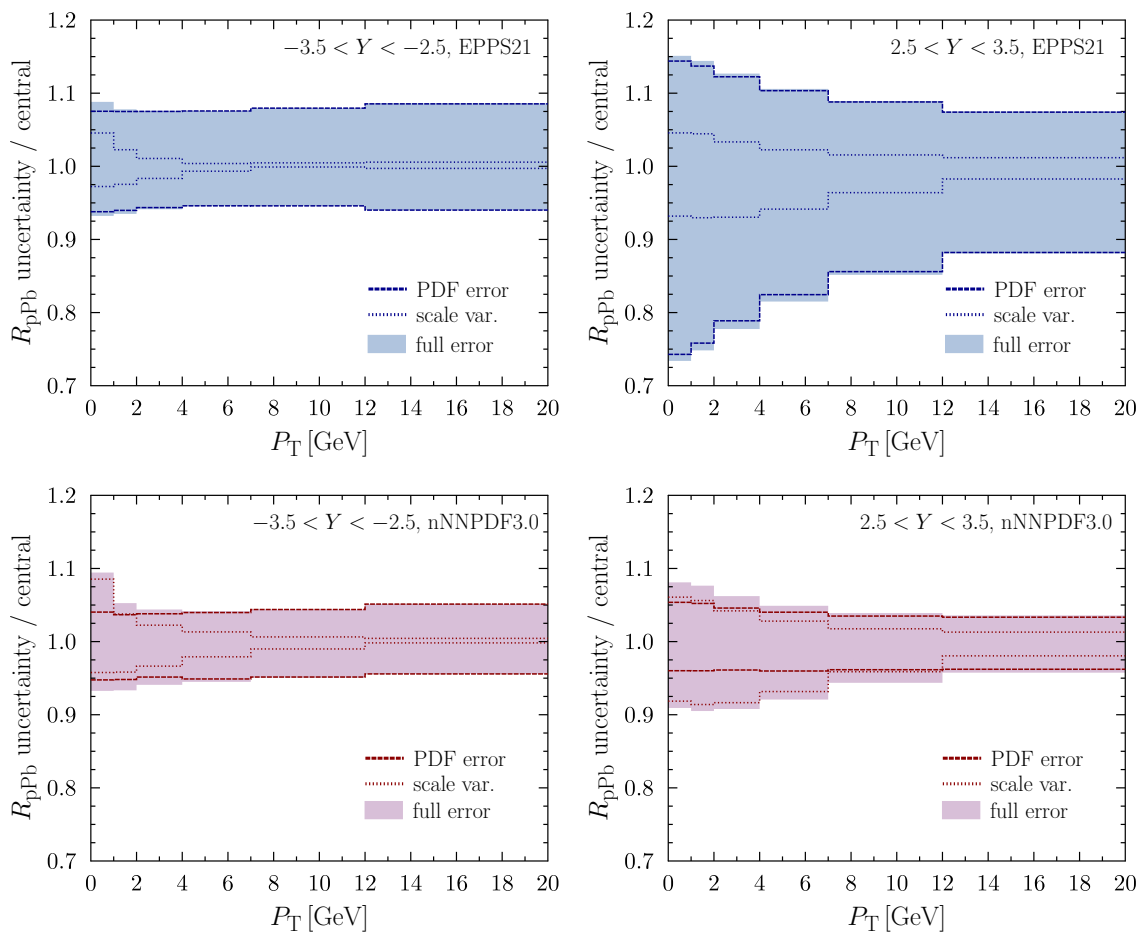
Figure 9. The scale (dotted) and 90% PDF (dashed) uncertainties of the B-meson nuclear modification factors in p-Pb collisions. The upper panels correspond to the EPPS21 PDFs [62] and the lower panels to the nNNPDF3.0 [63] PDFs.

enhancement (antishadowing) in comparison to the proton PDFs. In the forward direction $2.5 < Y < 3.5$ it is the small-x regime of nuclear PDFs that matters the most where the nuclear PDFs are suppressed (shadowing) in comparison to the proton PDFs. The LHCb data are broadly consistent with these expectations and quantitatively agree with both EPPS21 and nNNPDF3.0. In particular, the data at forward direction are more precise than the EPPS21 predictions and could possibly give some additional constraints in a global analysis of nuclear PDFs, though the statistical weight of these B-meson data will be small in a global χ^2 analysis. The lower panel still shows the forward-to-backward ratio

$$R_{\rm FB} = \frac{d^2\sigma^{\rm p\text{-}Pb}(Y>0)/dY dP_{\rm T}}{d^2\sigma^{\rm p\text{-}Pb}(Y<0)/dY dP_{\rm T}}, \qquad (4.2)$$

which requires no p-p baseline measurement. We also show the B^0 measurement — our calculation is identical for $B^{\pm}$ and B^0 (the KKSS08 FFs are the same for these two species). Note that the data in the forward and backward directions come from separate LHC runs with different beam configurations so the luminosity uncertainties do not cancel. Our
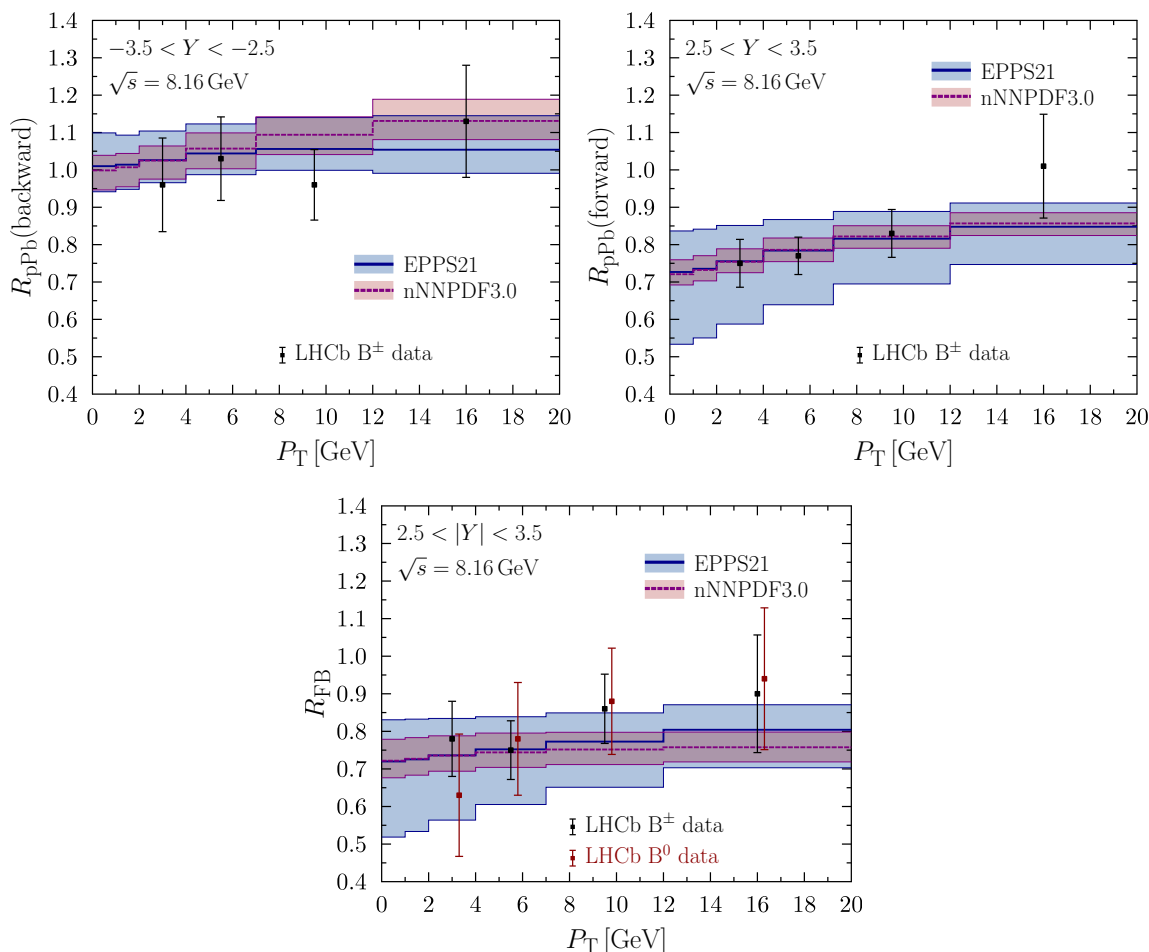
Figure 10. The nuclear modification factors (upper panels) and the forward-to-backward ratio (lower panel) for B mesons. The coloured bands correspond to the EPPS21 [62] (blue) and nNNPDF3.0 [63] (purple) nuclear-PDF uncertainties. The data are from ref. [34].

predictions are found to agree with the data also here. The data perhaps hints towards a stronger P_T dependence but a more precise measurement is still required to confirm this in a statistically significant way as notable fluctuations are seen in LHCb data for R_{pPb} at this P_T region.

5 Conclusion and outlook

In summary, we have extended the NLO SACOT-m_T scheme, originally introduced in the context of D-meson production, to the case of B-meson production at the LHC. In the original version we had defined a fragmentation variable that could lead to a pathological behaviour in certain corners of the phase space — a better version introduced in the present paper evades this problem. We contrasted our calculations against the proton-proton data from the LHCb, ATLAS and CMS collaborations finding a very good agreement within theoretical uncertainties originating from the variations of the renormalization/factorization/fragmentation scales and the bottom-quark mass. Notably, the shift

in the position of the peak value in P_{T} spectra when increasing the heavy-quark mass is naturally reproduced with our default setup. We found a good agreement also with the data at high-P_{T} region where the scale variations play a smaller role. To get some more insight on different GM-VFNS schemes, we compared our results to the FONLL approach and concluded that the somewhat different evolution of scale uncertainties as a function of P_{T} can be attributed to a different regulation of massless coefficient functions which also controls the relative contribution of direct and non-direct production channels. While the scale uncertainties can be large in the case of absolute cross sections, they are strongly suppressed e.g. in ratios of cross sections between different c.m. energies or ratios between different collision systems, which are then much more sensitive to the underlying proton and/or nuclear structure. In particular, we considered the nuclear modification R_{pPb} and the forward-to-backward ratio R_{FB} by using the EPPS21 and nNNPDF3.0 nuclear PDFs. The predictions agree very well with the data from the LHCb collaboration, lending further support for the universality of nuclear PDFs.

Having now tested the SACOT-m_{T} scheme in the case of inclusive D- and B-meson production, we plan to extend our framework also to include the decays of these open heavy flavours. In many cases the decay particles — e.g. the J/ψ spectrum from B mesons — can be measured with a significantly greater accuracy than the fully reconstructed D or B mesons. This would then open e.g. the possibility to include the corresponding R_{pPb} data to the global fits of nuclear PDFs without resorting to simplifying approximations made in other works and provide more constraints for small-x gluon shadowing in heavy nuclei. In addition, now that the fixed-order NNLO calculations for $b\bar{b}$ production are/will soon be publicly available, it begins to be possible to increase the accuracy of GM-VFNS in hadroproduction to include higher-order perturbative contributions.

Acknowledgments

References

[1] B.L. Combridge, *Associated Production of Heavy Flavor States in pp and p̄p Interactions: Some QCD Estimates*, [*Nucl. Phys. B* **151** (1979) 429](#) [[INSPIRE](#)].

[2] W. Beenakker, H. Kuijf, W.L. van Neerven and J. Smith, *QCD Corrections to Heavy Quark Production in pp̄ Collisions*, [*Phys. Rev. D* **40** (1989) 54](#) [[INSPIRE](#)].

[3] P. Nason, S. Dawson and R.K. Ellis, *The One Particle Inclusive Differential Cross-Section for Heavy Quark Production in Hadronic Collisions*, *Nucl. Phys. B* **327** (1989) 49 [INSPIRE].

[4] M. Czakon, P. Fiedler and A. Mitov, *Total Top-Quark Pair-Production Cross Section at Hadron Colliders Through $O(\alpha_S^4)$*, *Phys. Rev. Lett.* **110** (2013) 252004 [arXiv:1303.6254] [INSPIRE].

[5] S. Catani et al., *Bottom-quark production at hadron colliders: fully differential predictions in NNLO QCD*, *JHEP* **03** (2021) 029 [arXiv:2010.11906] [INSPIRE].

[6] S.J. Brodsky, P. Hoyer, C. Peterson and N. Sakai, *The Intrinsic Charm of the Proton*, *Phys. Lett. B* **93** (1980) 451 [INSPIRE].

[7] NNPDF collaboration, *Evidence for intrinsic charm quarks in the proton*, *Nature* **608** (2022) 483 [arXiv:2208.08372] [INSPIRE].

[8] M. Guzzi et al., *The persistent nonperturbative charm enigma*, *Phys. Lett. B* **843** (2023) 137975 [arXiv:2211.01387] [INSPIRE].

[9] F. Lyonnet et al., *On the intrinsic bottom content of the nucleon and its impact on heavy new physics at the LHC*, *JHEP* **07** (2015) 141 [arXiv:1504.05156] [INSPIRE].

[10] S. Forte, T. Giani and D. Napoletano, *Fitting the b-quark PDF as a massive-b scheme: Higgs production in bottom fusion*, *Eur. Phys. J. C* **79** (2019) 609 [arXiv:1905.02207] [INSPIRE].

[11] M. Cacciari, M.L. Mangano and P. Nason, *Gluon PDF constraints from the ratio of forward heavy-quark production at the LHC at $\sqrt{S} = 7$ and 13 TeV*, *Eur. Phys. J. C* **75** (2015) 610 [arXiv:1507.06197] [INSPIRE].

[12] R. Gauld, J. Rojo, L. Rottoli and J. Talbert, *Charm production in the forward region: constraints on the small-x gluon and backgrounds for neutrino astronomy*, *JHEP* **11** (2015) 009 [arXiv:1506.08025] [INSPIRE].

[13] K.J. Eskola, I. Helenius, P. Paakkinen and H. Paukkunen, *A QCD analysis of LHCb D-meson data in p+Pb collisions*, *JHEP* **05** (2020) 037 [arXiv:1906.02512] [INSPIRE].

[14] A. Kusina, J.-P. Lansberg, I. Schienbein and H.-S. Shao, *Reweighted nuclear PDFs using heavy-flavor production data at the LHC*, *Phys. Rev. D* **104** (2021) 014010 [arXiv:2012.11462] [INSPIRE].

[15] S. Bailey et al., *Parton distributions from LHC, HERA, Tevatron and fixed target data: MSHT20 PDFs*, *Eur. Phys. J. C* **81** (2021) 341 [arXiv:2012.04684] [INSPIRE].

[16] NNPDF collaboration, *The path to proton structure at 1% accuracy*, *Eur. Phys. J. C* **82** (2022) 428 [arXiv:2109.02653] [INSPIRE].

[17] T.-J. Hou et al., *New CTEQ global analysis of quantum chromodynamics with high-precision data from the LHC*, *Phys. Rev. D* **103** (2021) 014013 [arXiv:1912.10053] [INSPIRE].

[18] CMS collaboration, *Measurement of the double-differential inclusive jet cross section in proton-proton collisions at $\sqrt{s} = 13$ TeV*, *Eur. Phys. J. C* **76** (2016) 451 [arXiv:1605.04436] [INSPIRE].

[19] ALICE collaboration, *Measurements of inclusive jet spectra in pp and central Pb-Pb collisions at $\sqrt{s_{\mathrm{NN}}} = 5.02$ TeV*, *Phys. Rev. C* **101** (2020) 034911 [arXiv:1909.09718] [INSPIRE].

[20] ALICE collaboration, *$W^{\pm}$-boson production in $p-Pb$ collisions at $\sqrt{s_{NN}} = 8.16$ TeV and PbPb collisions at $\sqrt{s_{NN}} = 5.02$ TeV*, *JHEP* **05** (2023) 036 [arXiv:2204.10640] [INSPIRE].

[21] CMS collaboration, *Measurement of the $B^{\pm}$ Meson Nuclear Modification Factor in Pb-Pb Collisions at $\sqrt{s_{NN}} = 5.02$ TeV, Phys. Rev. Lett.* **119** (2017) 152301 [`arXiv:1705.04727`] [ɪɴSPIRE].

[22] CDF collaboration, *Measurement of the J/ψ meson and b-hadron production cross sections in $p\bar{p}$ collisions at $\sqrt{s} = 1960$ GeV, Phys. Rev. D* **71** (2005) 032001 [`hep-ex/0412071`] [ɪɴSPIRE].

[23] CDF collaboration, *Measurement of the B+ production cross-section in p anti-p collisions at $\sqrt{s} = 1960$ GeV, Phys. Rev. D* **75** (2007) 012010 [`hep-ex/0612015`] [ɪɴSPIRE].

[24] CMS collaboration, *Measurement of the B^0 production cross section in pp Collisions at $\sqrt{s} = 7$ TeV, Phys. Rev. Lett.* **106** (2011) 252001 [`arXiv:1104.2892`] [ɪɴSPIRE].

[25] CMS collaboration, *Measurement of the B^+ Production Cross Section in pp Collisions at $\sqrt{s} = 7$ TeV, Phys. Rev. Lett.* **106** (2011) 112001 [`arXiv:1101.0131`] [ɪɴSPIRE].

[26] CMS collaboration, *Measurement of the Strange B Meson Production Cross Section with $J/Psi \phi$ Decays in pp Collisions at $\sqrt{s} = 7$ TeV, Phys. Rev. D* **84** (2011) 052008 [`arXiv:1106.4048`] [ɪɴSPIRE].

[27] LHCʙ collaboration, *Measurement of the $B^{\pm}$ production cross-section in pp collisions at $\sqrt{s} = 7$ TeV, JHEP* **04** (2012) 093 [`arXiv:1202.4812`] [ɪɴSPIRE].

[28] LHCʙ collaboration, *Measurement of B meson production cross-sections in proton-proton collisions at $\sqrt{s} = 7$ TeV, JHEP* **08** (2013) 117 [`arXiv:1306.3663`] [ɪɴSPIRE].

[29] ATLAS collaboration, *Measurement of the differential cross-section of B^+ meson production in pp collisions at $\sqrt{s} = 7$ TeV at ATLAS, JHEP* **10** (2013) 042 [`arXiv:1307.0126`] [ɪɴSPIRE].

[30] CMS collaboration, *Measurement of the total and differential inclusive B^+ hadron cross sections in pp collisions at $\sqrt{s} = 13$ TeV, Phys. Lett. B* **771** (2017) 435 [`arXiv:1609.00873`] [ɪɴSPIRE].

[31] LHCʙ collaboration, *Measurement of the b-quark production cross-section in 7 and 13 TeV pp collisions, Phys. Rev. Lett.* **118** (2017) 052002 [*Erratum ibid.* **119** (2017) 169901] [`arXiv:1612.05140`] [ɪɴSPIRE].

[32] LHCʙ collaboration, *Measurement of the $B^{\pm}$ production cross-section in pp collisions at $\sqrt{s} = 7$ and 13 TeV, JHEP* **12** (2017) 026 [`arXiv:1710.04921`] [ɪɴSPIRE].

[33] CMS collaboration, *Study of B Meson Production in p+Pb Collisions at $\sqrt{s_{NN}} = 5.02$ TeV Using Exclusive Hadronic Decays, Phys. Rev. Lett.* **116** (2016) 032301 [`arXiv:1508.06678`] [ɪɴSPIRE].

[34] LHCʙ collaboration, *Measurement of B^+, B^0 and Λ_b^0 production in pPb collisions at $\sqrt{s_N N} = 8.16$ TeV, Phys. Rev. D* **99** (2019) 052011 [`arXiv:1902.05599`] [ɪɴSPIRE].

[35] R.S. Thorne and W.K. Tung, *PQCD Formulations with Heavy Quark Masses and Global Analysis*, in the proceedings of the *HERA and the LHC: 4th Workshop on the Implications of HERA for LHC Physics*, Geneva Switzerland, May 26–30 (2008), p. 332–351 [`arXiv:0809.0714`] [ɪɴSPIRE].

[36] M. Cacciari, M. Greco and P. Nason, *The P_T spectrum in heavy flavor hadroproduction, JHEP* **05** (1998) 007 [`hep-ph/9803400`] [ɪɴSPIRE].

[37] B.A. Kniehl, G. Kramer, I. Schienbein and H. Spiesberger, *Inclusive $D^{\pm}$ production in $p\bar{p}$ collisions with massive charm quarks, Phys. Rev. D* **71** (2005) 014018 [`hep-ph/0410289`] [ɪɴSPIRE].

[38] B.A. Kniehl, G. Kramer, I. Schienbein and H. Spiesberger, *Collinear subtractions in hadroproduction of heavy quarks*, *Eur. Phys. J. C* **41** (2005) 199 [hep-ph/0502194] [INSPIRE].

[39] B.A. Kniehl, G. Kramer, I. Schienbein and H. Spiesberger, *Finite-mass effects on inclusive B meson hadroproduction*, *Phys. Rev. D* **77** (2008) 014011 [arXiv:0705.4392] [INSPIRE].

[40] B.A. Kniehl, G. Kramer, I. Schienbein and H. Spiesberger, *Inclusive B-Meson Production at the LHC in the GM-VFN Scheme*, *Phys. Rev. D* **84** (2011) 094026 [arXiv:1109.2472] [INSPIRE].

[41] B.A. Kniehl, G. Kramer, I. Schienbein and H. Spiesberger, *Inclusive B-meson production at small p_T in the general-mass variable-flavor-number scheme*, *Eur. Phys. J. C* **75** (2015) 140 [arXiv:1502.01001] [INSPIRE].

[42] G. Kramer and H. Spiesberger, *b-hadron production in the general-mass variable-flavour-number scheme and LHC data*, *Phys. Rev. D* **98** (2018) 114010 [arXiv:1809.04297] [INSPIRE].

[43] M. Benzke et al., *B-meson production in the general-mass variable-flavour-number scheme and LHC data*, *Eur. Phys. J. C* **79** (2019) 814 [arXiv:1907.12456] [INSPIRE].

[44] I. Helenius and H. Paukkunen, *Revisiting the D-meson hadroproduction in general-mass variable flavour number scheme*, *JHEP* **05** (2018) 196 [arXiv:1804.03557] [INSPIRE].

[45] M. Guzzi, P.M. Nadolsky, H.-L. Lai and C.-P. Yuan, *General-Mass Treatment for Deep Inelastic Scattering at Two-Loop Accuracy*, *Phys. Rev. D* **86** (2012) 053005 [arXiv:1108.5112] [INSPIRE].

[46] K. Xie, *Massive elementary particles in the Standard Model and its supersymmetric triplet Higgs extension*, Ph.D. thesis, Department of Physics, Southern Methodist University, Dallas, U.S.A (2019) [INSPIRE].

[47] K. Xie, J.M. Campbell and P.M. Nadolsky, *A general-mass scheme for prompt charm production at hadron colliders*, *SciPost Phys. Proc.* **8** (2022) 084 [arXiv:2108.03741] [INSPIRE].

[48] P. Nason, *A New method for combining NLO QCD with shower Monte Carlo algorithms*, *JHEP* **11** (2004) 040 [hep-ph/0409146] [INSPIRE].

[49] S. Frixione, P. Nason and C. Oleari, *Matching NLO QCD computations with Parton Shower simulations: the POWHEG method*, *JHEP* **11** (2007) 070 [arXiv:0709.2092] [INSPIRE].

[50] S. Alioli, P. Nason, C. Oleari and E. Re, *A general framework for implementing NLO calculations in shower Monte Carlo programs: the POWHEG BOX*, *JHEP* **06** (2010) 043 [arXiv:1002.2581] [INSPIRE].

[51] J. Mazzitelli, A. Ratti, M. Wiesemann and G. Zanderighi, *B-hadron production at the LHC from bottom-quark pair production at NNLO+PS*, arXiv:2302.01645 [INSPIRE].

[52] S. Albino, B.A. Kniehl and G. Kramer, *AKK Update: Improvements from New Theoretical Input and Experimental Data*, *Nucl. Phys. B* **803** (2008) 42 [arXiv:0803.2768] [INSPIRE].

[53] F. Aversa, P. Chiappetta, M. Greco and J.P. Guillet, *QCD Corrections to Parton-Parton Scattering Processes*, *Nucl. Phys. B* **327** (1989) 105 [INSPIRE].

[54] B. Mele and P. Nason, *The Fragmentation function for heavy quarks in QCD*, *Nucl. Phys. B* **361** (1991) 626 [INSPIRE].

[55] K. Melnikov and A. Mitov, *Perturbative heavy quark fragmentation function through $\mathcal{O}(\alpha_s^2)$*, *Phys. Rev. D* **70** (2004) 034027 [hep-ph/0404143] [INSPIRE].

[56] J.C. Collins, F. Wilczek and A. Zee, *Low-Energy Manifestations of Heavy Particles: Application to the Neutral Current*, *Phys. Rev. D* **18** (1978) 242 [INSPIRE].

[57] SLD collaboration, *Measurement of the b quark fragmentation function in Z^0 decays*, *Phys. Rev. D* **65** (2002) 092006 [*Erratum ibid.* **66** (2002) 079905] [hep-ex/0202031] [INSPIRE].

[58] OPAL collaboration, *Inclusive analysis of the b quark fragmentation function in Z decays at LEP*, *Eur. Phys. J. C* **29** (2003) 463 [hep-ex/0210031] [INSPIRE].

[59] ALEPH collaboration, *Study of the fragmentation of b quarks into B mesons at the Z peak*, *Phys. Lett. B* **512** (2001) 30 [hep-ex/0106051] [INSPIRE].

[60] M. Czakon, T. Generet, A. Mitov and R. Poncelet, *NNLO B-fragmentation fits and their application to $t\bar{t}$ production and decay at the LHC*, *JHEP* **03** (2023) 251 [arXiv:2210.06078] [INSPIRE].

[61] T. Cridge, L.A. Harland-Lang, A.D. Martin and R.S. Thorne, *An investigation of the α_S and heavy quark mass dependence in the MSHT20 global PDF analysis*, *Eur. Phys. J. C* **81** (2021) 744 [arXiv:2106.10289] [INSPIRE].

[62] K.J. Eskola, P. Paakkinen, H. Paukkunen and C.A. Salgado, *EPPS21: a global QCD analysis of nuclear PDFs*, *Eur. Phys. J. C* **82** (2022) 413 [arXiv:2112.12462] [INSPIRE].

[63] R. Abdul Khalek et al., *nNNPDF3.0: evidence for a modified partonic structure in heavy nuclei*, *Eur. Phys. J. C* **82** (2022) 507 [arXiv:2201.12363] [INSPIRE].

[64] LHCB collaboration, *Measurements of prompt charm production cross-sections in pp collisions at $\sqrt{s} = 13$ TeV*, *JHEP* **03** (2016) 159 [*Erratum ibid.* **09** (2016) 013] [arXiv:1510.01707] [INSPIRE].

[65] M. Cacciari et al., *Theoretical predictions for charm and bottom production at the LHC*, *JHEP* **10** (2012) 137 [arXiv:1205.6344] [INSPIRE].

[66] M. Cacciari, *The FONLL Web interface*, http://www.lpthe.jussieu.fr/~cacciari/fonll/fonllform.html.

[67] NNPDF collaboration, *Parton distributions for the LHC Run II*, *JHEP* **04** (2015) 040 [arXiv:1410.8849] [INSPIRE].

[68] LHCB collaboration, *Study of prompt D^0 meson production in pPb collisions at $\sqrt{s_{NN}} = 5$ TeV*, *JHEP* **10** (2017) 090 [arXiv:1707.02750] [INSPIRE].

[69] C. Bierlich et al., *A comprehensive guide to the physics and usage of PYTHIA 8.3*, arXiv:2203.11601 [DOI:10.21468/SciPostPhysCodeb.8] [INSPIRE].

[70] P. Duwentäster et al., *Impact of heavy quark and quarkonium data on nuclear gluon PDFs*, *Phys. Rev. D* **105** (2022) 114043 [arXiv:2204.09982] [INSPIRE].

[71] A. Courtoy et al., *Parton distributions need representative sampling*, *Phys. Rev. D* **107** (2023) 034008 [arXiv:2205.10444] [INSPIRE].